

B 8 Phase behavior of colloidal systems

Christos N. Likos

Institute for Theoretical Physics II: Soft Matter

Heinrich-Heine-Universität Düsseldorf

Universitätsstraße 1, D-40225 Düsseldorf

Germany

Contents

1	Introduction: colloids and soft matter	2
2	The coarse-graining strategy: effective interactions	3
3	Classical uniform fluids	5
4	Nonuniform fluids: density functional theory (DFT)	9
4.1	The basic principles of DFT	9
4.2	Accurate density functionals for soft potentials	12
4.3	Fluid-fluid interfaces	13
4.4	Wetting	17
4.5	Crystallization	21
5	Summary and conclusions	23
A	Functionals and functional differentiation	23

1 Introduction: colloids and soft matter

Perhaps the most fascinating aspect of soft matter science lies in the fact that the physical systems considered in this field are not atomic or molecular in nature: the constituent particles of what are synonymously known as *complex fluids* are instead macromolecular aggregates, whose spatial extent lies in the domain between 1 nm and 1 μm . Although there is an abundance of naturally occurring soft matter systems (one only needs to think about proteins, viruses, and DNA molecules), a large variety of complex fluids are man-made [1,2]. It is hardly exaggerated to state that the overwhelming majority of the products of the food, pharmaceutical, detergent and chemical industries are indeed complex fluids. Therefore, there is an overwhelming need for an understanding of the mechanisms by which the physical characteristics of the constituting particles of the fluid are having an influence on the macroscopic properties of the physical system. This is indeed the central question of the field of statistical physics (equilibrium or otherwise): *Given a collection of a huge number of microscopic particles under a small number of fixed external parameters, which are the properties of the macroscopic system?* The question is hard enough to answer even when the constituent particles are simple atoms; the degree of difficulty increases by at least one order of magnitude in the case of complex fluids, in which the *internal* architecture and fluctuations of the aggregates play an additional role. But this challenging problem offers at the same time a chance to design new materials with unusual structural and rheological properties: only in the field of soft matter do we possess the possibility of changing the properties of the constituent particles externally. For atomic fluids, the particles are nature-given and the freedom to influence their interactions is absent.

A particular category of soft matter systems are known under the name *colloidal suspensions*; membranes, block copolymer melts, networks of filaments are other ones in the long list. Originally, the term *colloids* was employed to describe spherical, rigid particles of mesoscopic dimensions, i.e., *hard* colloids dispersed in a microscopic solvent. Examples of such particles are chemically synthesized polystyrene [3, 4], silica [5, 6] or poly-methyl-methacrylate (PMMA) particles [7, 8] that serve as realizations of hard-sphere solutions [9] or charge-stabilized colloidal suspensions, which have long attracted the interest of theorists and experimentalists alike [9–11]. Aspherical rigid particles, such as rods or platelets are also described under the name “colloids”, whereas recently the term has been extended to also include also soft particles (polymer chains, polyelectrolytes, star polymers, dendrimers) with mesoscopic dimensions. In this contribution we offer an overview of the theoretical tools employed with the goal of describing and understanding the structural and thermodynamic properties of these complex systems and the connections that can be made to experimentally measurable quantities. In view of the complexity of the solvent/solute system and the vast discrepancy in the length- and time-scales associated with the two components, a coarse-graining approach is necessary: a truly microscopic theory for such highly complex molecules would be prohibitively complicated. Therefore, we sketch the basic principles of the coarse-graining procedure in Section 2, in which we introduce, in particular, the concept of the *effective interaction* between complex macromolecular aggregates. In section 3 we turn our attention to the many-body problem of a *uniform* fluid made up of colloidal particles and to the current theoretical approaches employed to describe the fluid structure and thermodynamics. In section 4, we present the powerful tool of density functional theory, which offers the suitable theoretical framework for the description of *nonuniform* fluids and fluid interfaces. In section 5, we summarize and conclude. In the Appendix, we present a primer in the concept of a *functional* of a given function, in which the interested reader can also find an exposition to the rules of functional differentiation.

2 The coarse-graining strategy: effective interactions

Imagine that you want to visit the performance of a celebrated ballet ensemble, whose *prima ballerina* is world-famous for her extraordinary dancing skills. In this case, you would like to have a seating as close to the scene as possible, at a place where you can resolve every detail of the movement of the artists: the waving of their arms and the elegant, skillful motions of their legs and bodies are indeed important for obtaining the full aesthetic pleasure from the performance. Details of the motion in short length- and time-scales are relevant and quite a bit would be lost if one were seated at the last row, where just a diffuse ensemble of performers could be discerned. The situation is different if one wishes to attend the opening ceremony of the Olympic Games, for instance. Here, it is the *collective* behavior of a large number of individuals performing coordinated movements that matters. One is interested in seeing, from a more distant perspective, the large-scale shapes and patterns formed by the colorful groups of the performing individuals. The relevant motions take place at time scales that are longer than the ones involved in moving one's finger or arm; and the length scales of interest are correspondingly longer than the size of any single individual participating in the (literally!) many-body process. Here, a choice of first-row seating would be unwise. Much more would be gained if one positioned oneself farther away from the spectacle, so that the eyes automatically perform a 'coarse-graining' procedure of the event and the short scales get effortlessly eliminated from the view.

When dealing with soft matter systems, we are faced with a similar problem of coexistence of various different length- and time scales. Indeed, almost every complex fluid is a solution or dispersion of large particles in a molecular or atomic solvent. The solvent particles are much smaller and much faster than the dissolved ones. If, in addition, the solute particles are polymeric entities, there is a vast separation in the scales of the individual monomers and the aggregate as a whole. A choice has to be made, therefore, as to which kind of phenomena one is interested in. If the motions of the individual atoms are relevant, then a microscopic description of the system is of order. However, a host of interesting problems pertaining, e.g., to the overall phase or rheological behavior of the suspension, are rather connected to longer time scales and larger length scales. Small angle scattering experiments with thermal neutrons can hardly probe correlations at the monomer scale and they rather deliver information about the structure of the system at the *mesoscopic* scale. Optical tracer experiments probe the slow, diffusive motion of the macromolecular aggregates, in which the ultrafast motion of the individual atoms is lost. Accordingly, one would like to construct a theoretical tool that encaptures the coarse-graining procedure performed by such experiments: the small and fast degrees of freedom should be eliminated from the problem, with their influence being 'hidden' in the form or in the parameters of an interaction potential between the large and slow degrees of freedom only. This approach, of successful, also has the advantage of already performing the first step in bridging the scales: it takes us from the *microscopic* to the *mesoscopic* scale and the next step to the *macroscopic* domain is often not terribly complicated. Fig. 1 shows a sketch of the procedure specifically for the case of star polymers [12–14].

The coarse-graining procedure has its roots at the McMillan-Mayer theory of solutions [15] and its formulation by Kirkwood and Buff [16], for a review of its applications to colloids see the article by van Meegen and Snook [17]. The theoretical tool that expressed the coarse-graining at the mathematical level is called *effective interaction*. A detailed, statistical-mechanical description of the derivation of the effective interaction and its properties has been given, e.g., in Ref. [18]. Here we only sketch the main ideas of the procedure. Suppose that we are dealing

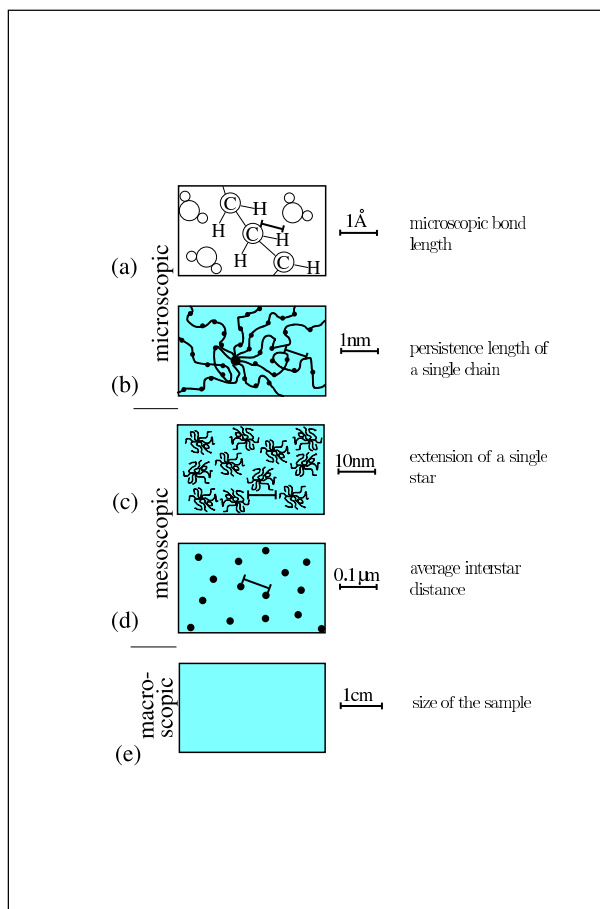


Fig. 1: The various length scales at which a star polymer solution can be looked upon, ranging from microscopic to macroscopic and covering in this way about eight orders of magnitude.

with a system whose Hamiltonian contains M ‘small’ degrees of freedom that are to be eliminated and N large ones that are to be kept. Let $V_{11}(\mathbf{r}^N)$ be the interaction potential between the large degrees of freedom, $V_{22}(\mathbf{s}^M)$ the one between the small ones and $V_{12}(\mathbf{r}^N, \mathbf{s}^M)$ the cross-interaction term, where $\{\mathbf{r}^N\}$ and $\{\mathbf{s}^M\}$ denote the coordinates of the large and small particles, respectively. The configurational part of the canonical partition function Z is given by

$$\begin{aligned} Z &= \int d\mathbf{r}^N \int d\mathbf{s}^M \exp \{ -\beta [V_{11}(\mathbf{r}^N) + V_{12}(\mathbf{r}^N, \mathbf{s}^M) + V_{22}(\mathbf{s}^M)] \} \\ &= \int d\mathbf{r}^N \exp [-\beta V_{11}(\mathbf{r}^N)] \int d\mathbf{s}^M \exp \{ -\beta [V_{12}(\mathbf{r}^N, \mathbf{s}^M) + V_{22}(\mathbf{s}^M)] \} \\ &= \int d\mathbf{r}^N \exp [-\beta V_{11}(\mathbf{r}^N)] \tilde{Z}(\mathbf{r}^N), \end{aligned} \quad (1)$$

where $\beta = (k_B T)^{-1}$, k_B denoting Boltzmann’s constant and T the absolute temperature, and $\tilde{Z}(\mathbf{r}^N)$ is, evidently, the constrained partition function of the small particles under a given configuration $\{\mathbf{r}^N\}$ of the big ones. By defining the corresponding constrained free energy $\tilde{F}(\mathbf{r}^N)$ as

$$\tilde{F}(\mathbf{r}^N) = -k_B T \ln \tilde{Z}(\mathbf{r}^N) \quad (2)$$

and the *effective interaction potential function* $V_{\text{eff}}(\mathbf{r}^N)$ as

$$V_{\text{eff}}(\mathbf{r}^N) = V_{11}(\mathbf{r}^N) + \tilde{F}(\mathbf{r}^N), \quad (3)$$

it is evident from eqs. (1)-(3) above that the partition function of the system can be expressed as a trace over the position coordinates of the large particles only and reads as

$$Z = \int d\mathbf{r}^N \exp [-\beta V_{\text{eff}}(\mathbf{r}^N)]. \quad (4)$$

An unavoidable consequence of the partial trace is that the effective Hamiltonian contains not only pair interactions but also the whole sequence of many-body forces. An explicit, diagrammatic expansion in the semi-grand ensemble that brings about the structure of the many-body terms has been carried out in Ref. [19]. Usually, however, the pair-potential approximation is employed and indeed there are only few cases for which this has proven inadequate. In other words, we express the effective interaction potential as a sum of pair interactions, explicitly

$$V_{\text{eff}}(\mathbf{r}^N) = \sum_{i < j} v_{\text{eff}}(|\mathbf{r}_i - \mathbf{r}_j|), \quad (5)$$

where $\mathbf{r}_{i,j}$ denote the positions of the i, j -particle. Furthermore, there is an overall extensive and coordinate-independent term in the effective Hamiltonian that also derives from the above-mentioned procedure. This so-called ‘volume term’ does not influence the correlation functions of the large particles, though, that remain unaffected by the procedure of deriving the effective interaction. It does influence the total thermodynamics, however, so care must be taken in treatments regarding, e.g., phase equilibria [19–21].

3 Classical uniform fluids

The translational invariance of \mathcal{H}_{eff} implies that the one-particle density of the system is a position-independent constant which is simply equal to the average particle density. In the absence of spontaneous symmetry breaking, the physical state of the system is also translationally

invariant and we are dealing with a uniform fluid of density ρ :

$$\rho^{(1)}(\mathbf{r}) = \rho = \frac{N}{V}, \quad (6)$$

where N stands for the number of particles enclosed in the macroscopic volume V .¹ Accordingly, in a fluid, the two-particle density depends only on the magnitude of the difference of its arguments:

$$\rho^{(2)}(\mathbf{r}, \mathbf{r}') = \rho^{(2)}(|\mathbf{r} - \mathbf{r}'|). \quad (7)$$

In the theory of classical fluids, a quantity of central importance for the investigation of the pair structure of the system is the radial distribution function $g(|\mathbf{r} - \mathbf{r}'|)$ defined through:

$$\rho^{(2)}(|\mathbf{r} - \mathbf{r}'|) = \rho^2 g(|\mathbf{r} - \mathbf{r}'|). \quad (8)$$

Physically, the quantity $\rho g(|\mathbf{r} - \mathbf{r}'|)$ is proportional to the conditional probability density of finding a particle at position \mathbf{r}' given that another particle is located at position \mathbf{r} . The typical shape of $g(r)$ for a dense liquid is shown in Fig. 2(a).

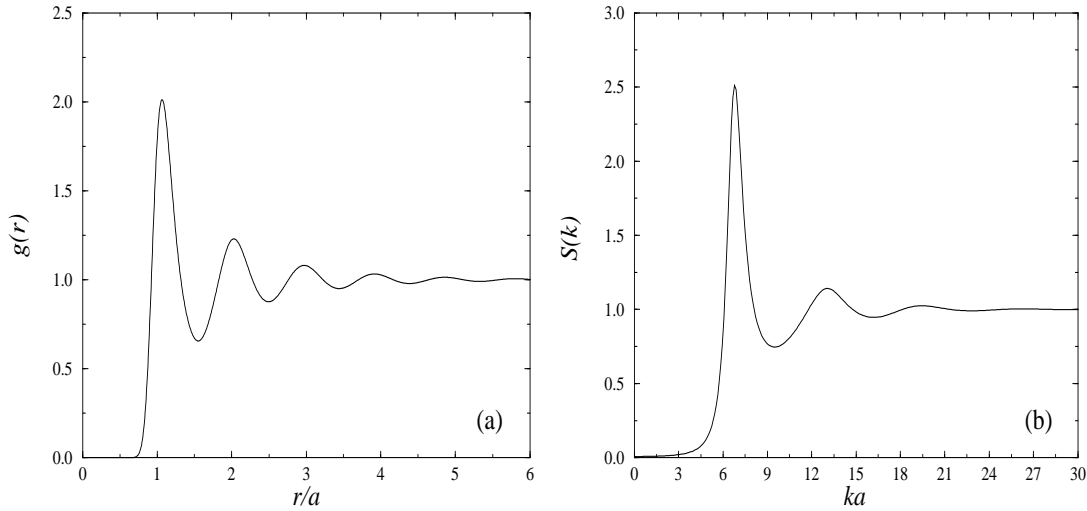


Fig. 2: Typical shapes of (a) the radial distribution function $g(r)$ and (b) the structure factor $S(k)$ of a dense, classical liquid. The length scale a is set by the density, $a = \rho^{-1/3}$. Notice the successive coordination shells in real space (represented by the maxima of the radial distribution function), reflecting the short-range order of the fluid state.

Another important quantity is the structure factor $S(k)$ of a fluid defined as a three-dimensional Fourier transform of the total correlation function $h(r) = g(r) - 1$:

$$S(k) = 1 + \rho \int d^3r h(r) e^{-i\mathbf{k} \cdot \mathbf{r}}, \quad (9)$$

which depends only on the magnitude k of the wavevector \mathbf{k} since $h(r)$ is a radially symmetric function.² A typical structure factor for a dense liquid is shown in Fig. 2(b). It can be

¹Unless explicitly stated otherwise, the *thermodynamic limit*, $N, V \rightarrow \infty$ with $N/V = \rho$, constant, will be assumed throughout.

²We denote the integration in $d = 3$ spatial coordinates but Eq. (9) as well as Eq. (11) that follows hold in arbitrary spatial dimensions.

shown [22] that the scattering intensity from a liquid sample at momentum transfer \mathbf{k} is proportional to $S(k)$. This makes the structure factor an important diagnostic tool for testing the accuracy of liquid-state theories, in which this quantity is usually calculated by means of some approximation.³ Moreover, the quantity $S(k)$ offers a path to thermodynamics, as its $k = 0$ value is proportional to the isothermal compressibility χ_T of the system [22]:

$$S(0) = \rho k_B T \chi_T. \quad (10)$$

For the theoretical approaches to the determination of the pair structure in the fluid state, one important function is the direct correlation function $c(r)$ connected to $h(r)$ through the *Ornstein-Zernike relation* which has the form:

$$h(r) = c(r) + \rho \int d^3r' c(|\mathbf{r} - \mathbf{r}'|) h(r'). \quad (11)$$

The Ornstein-Zernike relation is exact. As it connects two unknown functions, one more relation or *closure* is needed in order to determine $g(r)$ and $c(r)$. Closures are approximate relations which arise from exact diagrammatic expansions of $g(r)$ in terms of $c(r)$ but with certain classes of diagrams ignored. The exact relation between $g(r)$ and $c(r)$ reads as [22]

$$g(r) = \exp [-\beta v(r) + g(r) - 1 - c(r) + B(r)], \quad (12)$$

where $v(r)$ is the pair potential and $B(r)$ is the so-called *bridge function*, consisting of the sum of all elementary diagrams that are not nodal. The bridge function is of short range and rather insensitive to the detailed form of the pair potential [24]. All known closures can be thought of as approximate relations for the form of $B(r)$. Common closures are the Percus-Yevick (PY) and hypernetted chain (HNC) approximations [22]. In the PY closure, the approximation for $B(r)$ reads as

$$B_{\text{PY}}(r) = -[g(r) - c(r)] + 1 + \ln[g(r) - c(r)] \quad (\text{PY}), \quad (13)$$

whereas in the HNC the approximation is made that the bridge function vanishes:

$$B_{\text{HNC}}(r) = 0 \quad (\text{HNC}). \quad (14)$$

Eqs. (13) and (14) together with the exact relation (12) yield the common forms of the PY and HNC closures as

$$c(r) = g(r) [1 - e^{\beta v(r)}] \quad (\text{PY}) \quad (15)$$

and

$$g(r) = e^{-\beta v(r) + h(r) - c(r)} \quad (\text{HNC}). \quad (16)$$

The Ornstein-Zernike relation, supplied with a closure, leads to the determination of the quantities $c(r)$, $g(r)$ and $S(k)$ for a given interaction potential $v(r)$ and at given thermodynamic

³The scattering intensity is directly proportional to $S(k)$ only when we consider scattering from point particles. When we deal with large particles, such as colloids, then the form factor $P(k)$ of the particle has to be taken into account and the scattering intensity is proportional to the *product* $P(k)S(k)$ [23].

conditions, e.g., density and temperature. Various other quantities of interest, such as the pressure P or the energy U can be calculated as integrals involving the radial distribution function:

$$P = k_B T \rho - \frac{2\pi\rho^2}{3} \int_0^\infty r^3 v'(r) g(r) dr, \quad (17)$$

and

$$\frac{U}{N} = \frac{3k_B T}{2} + 2\pi\rho \int_0^\infty r^2 v(r) g(r) dr, \quad (18)$$

where $v'(r) = dv(r)/dr$. The free energy F can then be determined by thermodynamic integration of P (the *pressure route*) or of U (the *energy route*) as given in eqs. (17) and (18) above. A third possibility is to use eq. (10) and the thermodynamic definition of the isothermal compressibility, $\chi_T = (V\partial^2 F/\partial V^2)^{-1}$. This constitutes the *compressibility route*. If the *exact* radial distribution function $g(r)$ were known, then all three routes would yield identical results for the free energy. Due to the approximations in constructing a closure, however, this is not the case: every route yields a different free energy curve. This is the problem of *thermodynamic inconsistency* of the closure [22].

The procedure to obtain the structure and thermodynamics of translationally invariant systems (liquids and gases) described above, is known under the name *integral equation theories* (IET's). For every possible closure, one has to solve two coupled integral equations. There is by now a large variety of closures in the literature and the accuracy of a given closure depends sometimes on the characteristics of the interaction potential. For example, the PY closure is known to yield very accurate results for short-range, hard interactions, whereas the HNC is accurate for long-range, soft potentials [25].

The problem of thermodynamic inconsistency mentioned above is usually addressed by modifying the integral equation through the inclusion in the closure of a function which contains one or more additional parameters [24–28]. These parameters are then tuned until thermodynamic consistency is achieved, obtaining in this way not only the thermodynamics but also the pair structure with high accuracy. A particularly simple closure which yields excellent results for purely repulsive potentials was introduced by Rogers and Young [25] and reads as

$$g(r) = \exp[-\beta v(r)] \left[1 + \frac{\exp[\gamma(r)f(r)] - 1}{f(r)} \right], \quad (19)$$

where

$$\gamma(r) = h(r) - c(r) \quad (20)$$

and the function $f(r)$ is chosen to have the form

$$f(r) = 1 - \exp(-\alpha r). \quad (21)$$

Thermodynamic consistency is achieved by varying the parameter α . A comparison between eqs. (19), (21) and (15), (16) shows that the Rogers-Young closure reduces to the PY when $\alpha = 0$ and to the HNC when $\alpha = \infty$.

4 Nonuniform fluids: density functional theory (DFT)

4.1 The basic principles of DFT

In the preceding section, we discussed the pair structure and the thermodynamics of *homogeneous* fluids, also called *uniform* fluids, to emphasize the fact that their density is independent of the position. Of course, when we say ‘density’, we refer not to an instantaneous value but rather to a time- or ensemble average. The process of obtaining this quantity can be visualized as follows. Imagine dividing the whole space into increasingly small cells of volume ΔV and let $\Delta N(\mathbf{r})$ be the number of particles enclosed in the cell centered at the position \mathbf{r} . Consider the ratio $\Delta N(\mathbf{r})/\Delta V$ in the limit $\Delta V \rightarrow 0$ and take the ensemble average of it, $\langle \lim_{\Delta V \rightarrow 0} \Delta N(\mathbf{r})/\Delta V \rangle$. In a uniform fluid, the latter quantity is \mathbf{r} -independent and equal to the usual, homogeneous density ρ of the system. However, in many situations in condensed matter physics, the systems involved are spatially inhomogeneous, i.e., the density turns into a spatially-dependent field $\rho(\mathbf{r})$ in thermodynamic equilibrium.⁴ Typical examples are the nonuniform density profiles arising in phase-separated liquids or liquid mixtures, in fluids under the influence of external potentials (confining walls, optical-laser fields, electrostatic or magnetostatic fields) and, in the most extreme case, the vast inhomogeneities appearing when the translational symmetry of the system breaks and the fluid freezes into a crystalline solid. Density functional theory (DFT) is with a powerful tool to accurately analyze these situations and make nontrivial predictions on a number of properties of the physical systems under consideration.⁵

Let us start with a more precise definition of the (inhomogeneous) density $\rho(\mathbf{r})$. Consider a system of N pointlike particles of mass m in the volume V and let $\{\mathbf{r}_i\}$, $i = 1, 2, \dots, N$ be their positions and $\{\mathbf{p}_i\}$ their momenta. Suppose, without restriction to pair potentials, that $U(\{\mathbf{r}_i\})$ is the potential energy function describing their interactions and that the system is additionally placed under the influence of a one-body external potential $V_{\text{ext}}(\mathbf{r})$. The Hamiltonian $\hat{\mathcal{H}}_N$ for the N -body system is, therefore⁶

$$\hat{\mathcal{H}}_N(\mathbf{p}^N, \mathbf{r}^N) = \sum_{i=1}^N \frac{\mathbf{p}_i^2}{2m} + U(\mathbf{r}_1, \mathbf{r}_2, \dots, \mathbf{r}_N) + \sum_{i=1}^N V_{\text{ext}}(\mathbf{r}_i). \quad (22)$$

We employ the grand ensemble, in which the chemical potential μ is fixed and the particle number N is allowed to fluctuate, defining thereby the grand canonical partition function Ξ as

$$\Xi = \sum_{N=0}^{\infty} \frac{1}{h^{3N} N!} \int d\mathbf{p}^N \int d\mathbf{r}^N \exp[-\beta(\hat{\mathcal{H}}_N - \mu N)], \quad (23)$$

and the associated grand potential Ω as

$$\Omega(V, T, \mu) = -k_B T \ln \Xi. \quad (24)$$

⁴In the presence of time-dependent external fields, the one particle density becomes a spatiotemporal field $\rho(\mathbf{r}, t)$. Recent developments allow for the extension of DFT-approaches also to dynamical problems [29–36].

⁵Here, we will present a concise exposure to the principles of DFT, avoiding proofs of the theorems associated with it. For a more detailed discussion, we refer the reader to the standard work of R. Evans [37].

⁶In this section, we place a hat above the symbol of a classical operator $\hat{\mathcal{O}}$ that depends on the canonical variables of the system, in order to distinguish it from its thermodynamic average.

The expectation value of any operator $\hat{\mathcal{O}}(\mathbf{p}^N, \mathbf{r}^N)$ is given in this ensemble as

$$\mathcal{O} \equiv \langle \hat{\mathcal{O}}(\mathbf{p}^N, \mathbf{r}^N) \rangle = \frac{1}{\Xi} \sum_{N=0}^{\infty} \frac{1}{h^{3N} N!} \int d\mathbf{p}^N \int d\mathbf{r}^N \hat{\mathcal{O}}(\mathbf{p}^N, \mathbf{r}^N) \exp[-\beta(\hat{\mathcal{H}}_N - \mu N)]. \quad (25)$$

The so-called one-particle density operator $\hat{\rho}(\mathbf{r})$ is defined as

$$\hat{\rho}(\mathbf{r}) = \sum_{i=1}^N \delta(\mathbf{r} - \mathbf{r}_i), \quad (26)$$

and the one-particle density $\rho(\mathbf{r})$ is then nothing else but the expectation value of this operator in the sense of Eq. (25) above, namely

$$\rho(\mathbf{r}) = \langle \hat{\rho}(\mathbf{r}) \rangle. \quad (27)$$

Evidently, $\int d^d r \rho(\mathbf{r}) = \langle N \rangle$, with $\langle N \rangle$ denoting the expectation value of the particle number⁷ in the system for the given μ .

For a given interaction function $U(\{\mathbf{r}_i\})$ and fixed temperature T and chemical potential μ , the definitions above make it clear that $\rho(\mathbf{r})$ is *uniquely determined* by the external potential $V_{\text{ext}}(\mathbf{r})$. The key property that lends DFT its power lies in the fact that also the opposite is true: a given, equilibrium density profile $\rho_0(\mathbf{r})$ also uniquely determines the external potential $V_{\text{ext}}(\mathbf{r})$ that gives rise to it. The proof of this important theorem follows the lines of *reductio ad absurdum* and can be found in Ref. [37]. The implication is, then, that the grand potential Ω becomes a functional of $\rho_0(\mathbf{r})$, i.e., $\rho_0(\mathbf{r})$ uniquely determines the thermodynamics of the system.⁸ Taking into account Eqs. (22)-(27) above, we see that Ω can be expressed as

$$\Omega[\rho_0] = F[\rho_0] + \int d^d r [V_{\text{ext}}(\mathbf{r}) - \mu] \rho_0(\mathbf{r}), \quad (28)$$

where the *intrinsic free energy* $F[\rho_0]$ explicitly depends only on $\rho_0(\mathbf{r})$ and is, evidently, also a unique functional of the one-particle density. In interpreting Eq. (28) above, it must be kept in mind that the external potential $V_{\text{ext}}(\mathbf{r})$ that appears there is not arbitrary but rather precisely the external potential that gives rise to $\rho_0(\mathbf{r})$ as the equilibrium profile.

Motivated by the form of Eq. (28) above, we now introduce an extended functional $\tilde{\Omega}([\rho], [V_{\text{ext}}])$ of *both* $\rho(\mathbf{r})$ and $V_{\text{ext}}(\mathbf{r})$ as

$$\tilde{\Omega}([\rho], [V_{\text{ext}}]) = F[\rho] + \int d^d r [V_{\text{ext}}(\mathbf{r}) - \mu] \rho(\mathbf{r}). \quad (29)$$

Evidently, when $\rho(\mathbf{r}) = \rho_0(\mathbf{r})$, $\tilde{\Omega}([\rho_0], [V_{\text{ext}}]) = \Omega[\rho_0]$, the grand potential of the system and $F[\rho_0]$ becomes the intrinsic Helmholtz free energy of the same. The computational power associated with DFT comes from a variational principle, which states that $\tilde{\Omega}([\rho], [V_{\text{ext}}])$ attains its *minimum value* for the equilibrium density profile $\rho_0(\mathbf{r})$ [37]:

$$\tilde{\Omega}([\rho], [V_{\text{ext}}]) > \tilde{\Omega}([\rho_0], [V_{\text{ext}}]) \equiv \Omega[\rho_0] \text{ for } \rho(\mathbf{r}) \neq \rho_0(\mathbf{r}). \quad (30)$$

⁷We display all integrations in d -dimensional space, as the results of this section are general, and we will return to the familiar, $d = 3$ -space in practical examples that follow.

⁸For a crash-course on functionals and functional differentiation, see Appendix A.

The equilibrium density profile of a system, $\rho_0(\mathbf{r})$, can therefore be determined by minimizing $\tilde{\Omega}([\rho], [V_{\text{ext}}])$ with respect to $\rho(\mathbf{r})$, viz.

$$\left. \frac{\delta \tilde{\Omega}([\rho], [V_{\text{ext}}])}{\delta \rho(\mathbf{r})} \right|_{\rho(\mathbf{r})=\rho_0(\mathbf{r})} = 0, \quad (31)$$

or, using Eq. (29)

$$\left. \frac{\delta F[\rho]}{\delta \rho(\mathbf{r})} \right|_{\rho(\mathbf{r})=\rho_0(\mathbf{r})} = \mu - V_{\text{ext}}(\mathbf{r}). \quad (32)$$

The free energy functional $F[\rho]$ is hence the object of central interest in DFT. For each interaction potential there exists a unique functional $F[\rho]$ that determines the equilibrium configuration of the system under the influence of an arbitrary external potential $V_{\text{ext}}(\mathbf{r})$ with the help of Eq. (32). For noninteracting particles, we can write down this functional exactly. It is referred to as ‘ideal free energy’ $F_{\text{id}}[\rho]$ and it takes the form

$$F_{\text{id}}[\rho] = k_{\text{B}}T \int d^d r \rho(\mathbf{r}) \{ \ln [\rho(\mathbf{r})\Lambda^3] - 1 \}, \quad (33)$$

with the thermal de Broglie wavelength Λ . Application of the minimization principle, Eq. (32), to an ideal gas then leads to the equilibrium profile

$$\rho_0(\mathbf{r}) = \Lambda^{-3} \exp(\beta\mu) \exp[-\beta V_{\text{ext}}(\mathbf{r})], \quad (34)$$

which we recognize as a generalization of the barometric law.

For interacting systems it is customary to separate $F[\rho]$ into the ideal free energy contribution of Eq. (33) and the excess contribution $F_{\text{ex}}[\rho]$ arising from the interactions:

$$F[\rho] = F_{\text{id}}[\rho] + F_{\text{ex}}[\rho]. \quad (35)$$

The excess free energy is a generating functional for the direct correlation functions of n -th order, $c^{(n)}$, which are defined as

$$c^{(n)}(\mathbf{r}_1, \mathbf{r}_2, \dots, \mathbf{r}_n; [\rho]) = - \frac{\delta^n \beta F_{\text{ex}}[\rho]}{\delta \rho(\mathbf{r}_1) \delta \rho(\mathbf{r}_2) \cdots \delta \rho(\mathbf{r}_n)}. \quad (36)$$

The direct correlation function $c(r)$ of a fluid is precisely $c^{(2)}(\mathbf{r}_1, \mathbf{r}_2; [\rho])$ in the limit of a spatially homogeneous density field. In this case, the translational and rotational invariance of the underlying physical system imply that $c^{(2)}$ depends on \mathbf{r}_1 and \mathbf{r}_2 only through the combination $r \equiv |\mathbf{r}_1 - \mathbf{r}_2|$.

A great deal of effort has been devoted in the last thirty years, in order to construct approximate functionals $F_{\text{ex}}[\rho]$, at least for some model interaction potentials that can serve as a reference for more realistic ones. The pioneering work on the construction of approximate functionals is due to Ramakrishnan and Yussouff (RY) [38], who proposed a functional Taylor expansion of $F_{\text{ex}}[\rho]$ around the uniform fluid, truncated at the second order. The decisive merit of the RY-theory is its generality: it can be applied to any interacting system and the functional that ensues is generic in form, with the input dcf of the uniform fluid carrying the signature of the interaction potential. Improvements to the RY-approach were such developed, and mostly applied to the

hard-sphere system and its freezing transition. These come under the generic name of *weighted-density approximations*, for a review see Ref. [39]. A prominent example of a weighted density functional is the geometry-based *fundamental-measure theory* of Rosenfeld [40] and its subsequent extensions and generalizations to more complex systems [41]. There exists no reliable geometry-based, Rosenfeld-type functional for soft potentials, however, because the notion of a geometric shape is not well defined for a soft, deformable object.

4.2 Accurate density functionals for soft potentials

On the opposite extreme of the hard-sphere interaction potential lies the family of the *ultrasoft* interaction potentials $v(r)$. The latter can be generally defined through the property of *integrability*, which in three dimensions takes the form

$$\int_0^\infty r^2 v(r) dr < \infty. \quad (37)$$

Eq. (37) above is, evidently, not satisfied by the hard-sphere interaction and by the whole family of steeply diverging inverse-power-law potentials, $v(r) = \epsilon(\sigma/r)^m$. However, the Yukawa interaction, $v(r) = \epsilon \exp(-\lambda r)/(\lambda r)$, the Gaussian-like interactions between polymer coils [42], polyelectrolytes [43], and dendrimers in the center-of-mass representation [44–46], the interaction potentials between star polymers [13] and polymer chains in the midpoint representation [47], as well as the effective interactions between microgels [48, 49] and polyelectrolyte stars [50, 51] do belong to the class of ultrasoft potentials.

It has been shown [52–58] that for ultrasoft potentials a very simple and accurate functional for the excess free energy is provided by the so-called mean-field approximation (MFA) or random-phase approximation (RPA), namely:

$$F_{\text{ex}}[\rho] = \frac{1}{2} \int \int d^3x d^3y \rho(\mathbf{x}) \rho(\mathbf{y}) v(|\mathbf{x} - \mathbf{y}|). \quad (38)$$

The physical motivation behind Eq. (39) above lies in the absence of significant short-range correlations between the particles, caused by the ultrasoft divergence of $v(r)$ as $r \rightarrow 0$. Accordingly, one approximates the excess free energy of the system just by the interaction energy between the particles. It should be noted that Eq. (39) above becomes increasingly accurate as the density of the system grows, because in this case each particle interacts with an increasing number of other ones, thus justifying the mean-field character of the approximation. An implication of Eq. (39), in conjunction with Eq. (36), is the random-phase approximation for the direct correlation function $c(r)$, namely

$$c(r) = -\beta v(r). \quad (39)$$

The RPA functional can be easily generalized to a ν -component mixture of particles, mutually interacting through the *ultrasoft* pair potentials $v_{ij}(r)$ with $v_{ij}(r) = v_{ji}(r)$, $i, j = 1, 2, \dots, \nu$. The free energy functional F depends then on the ν density profiles $\rho_1(\mathbf{r}), \rho_2(\mathbf{r}), \dots, \rho_\nu(\mathbf{r})$ and takes the form [55]:

$$\begin{aligned} F[\{\rho_i\}] &= k_B T \sum_{i=1}^{\nu} \int d^3r \rho_i(\mathbf{r}) \{ \ln [\rho_i(\mathbf{r}) \Lambda_i^3] - 1 \} \\ &+ \frac{1}{2} \sum_{i=1}^{\nu} \sum_{j=1}^{\nu} \int \int d^3x d^3y \rho_i(\mathbf{x}) \rho_j(\mathbf{y}) v_{ij}(|\mathbf{x} - \mathbf{y}|), \end{aligned} \quad (40)$$

with the thermal de Broglie wavelength Λ_i or species i . The variational grand potential for a mixture is simply given by [cf. Eq. (29)]:

$$\tilde{\Omega}[\{\rho_i\}, \{V_{\text{ext}}^{(i)}\}] = F[\{\rho_i\}] + \sum_{i=1}^{\nu} \int d^3r \left[V_{\text{ext}}^{(i)}(\mathbf{r}) - \mu_i \right] \rho_i(\mathbf{r}), \quad (41)$$

where μ_i is the chemical potential of species i and $V_{\text{ext}}^{(i)}(\mathbf{r})$ the external potential acting on it. The equilibrium density profiles are then determined by the simultaneous solution of the ν coupled equations [cf. Eq. (31)]:

$$\frac{\delta \tilde{\Omega}[\{\rho_i\}, \{V_{\text{ext}}^{(i)}\}]}{\delta \rho_i(\mathbf{r})} = 0, \quad \text{for } i = 1, 2, \dots, \nu. \quad (42)$$

4.3 Fluid-fluid interfaces

Here we proceed to a specific application of DFT for an ultrasoft mixture, to provide a taste of the power and elegance of DFT-methods and of the RPA-functional in particular. Archer *et al.* [57] considered a binary mixture of athermal polymer chains. Taking the chains' midpoints as effective coordinates, they reduced the problem to a binary mixture of soft particles interacting by means of the pair potentials:

$$\beta v_{ij}(r) = \frac{5}{18} f^{3/2} \begin{cases} -\ln\left(\frac{r}{\sigma_{ij}}\right) + \frac{1}{2\tau_{ij}^2 \sigma_{ij}^2} & \text{for } r \leq \sigma_{ij}; \\ \frac{1}{2\tau_{ij}^2 \sigma_{ij}^2} \exp[-\tau_{ij}^2(r^2 - \sigma_{ij}^2)] & \text{for } r > \sigma_{ij}, \end{cases} \quad (43)$$

where σ_{ii} is the corona diameter and τ_{ii} is a parameter of order $1/R_{ii}$, with R_{ii} being the radius of gyration of species i [47] and $\beta = 1/k_B T$. Here, f represents, in general, the arm number of star polymers and we focus on $f = 2$, so that the star polymer pair potential (43) is equivalent to the effective potential between the central monomers on a polymer chain. For the 'cross-parameters' σ_{12} and τ_{12} , the 'mixing rules' employed read as

$$\sigma_{12} = \frac{1}{2}(\sigma_{11} + \sigma_{22}) \quad (44)$$

and

$$\frac{1}{\tau_{12}^2} = \frac{1}{2} \left(\frac{1}{\tau_{11}^2} + \frac{1}{\tau_{22}^2} \right). \quad (45)$$

In what follows, we will discuss results obtained using the interactions of Eq. (43) and the RPA-density functional of Eq. (40) for the case $\sigma_{22}/\sigma_{11} = 2^{-3/5}$ that corresponds to polymer mixtures of polymerization ratio $N_1 : N_2 = 2 : 1$, a standard test case.⁹

Setting $\rho_i(\mathbf{r}) = \rho_i$, $i = 1, 2$ in Eq. (40) immediately yields the Helmholtz free energy of the mixture, $F = Nf(\rho_1, \rho_2)$. A standard Legendre transformation leads then to the Gibbs free energy per particle, $g(x, P)$, where $x = \rho_2/(\rho_1 + \rho_2)$ is the concentration of species 2 and P the pressure. Stable, homogeneous mixtures are characterized by $g''(x) \geq 0$ for all x -values. The occurrence of concave parts in $g(x, P)$ signals a demixing transition with the coordinates of the coexisting phases given by the common tangent construction. The resulting phase diagram for the system is shown in Fig. 3 above, where it can be seen that the system shows a demixing transition at high densities.

⁹This arises from the scaling law $R \sim N^\nu$ connecting the spatial extent R of a self avoiding polymer with its degree of polymerization N , using the value $\nu = 3/5$ of the Flory exponent.

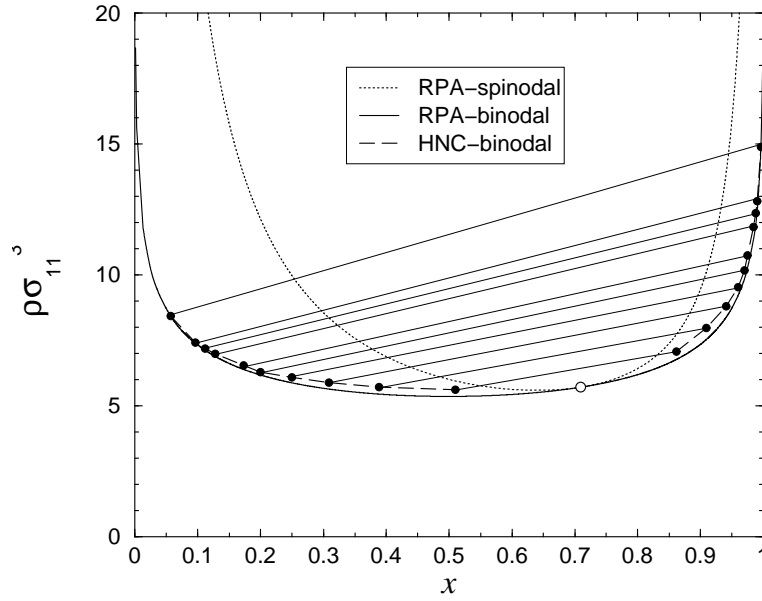


Fig. 3: The RPA-spinodal and binodal lines for the star-polymer mixture (dotted and solid lines) along with the HNC-binodal (dashed line). x is the concentration of species 2, the smaller component. The straight segments denote HNC-tielines between coexisting fluid phases whose coordinates are given by the closed circles at their ends. (From Ref. [57]).

The full power of DFT further develops when looking into more subtle, structural quantities in the bulk or at interfaces. Indeed, the form of the RPA-functional, implying $c_{ij}(r) = -\beta v_{ij}(r)$ allows for an explicit calculation of the complex poles of the structure factors of the two components. These, in turn, deliver information about the decay of the correlation functions $g_{ij}(r)$ in the bulk system for large r -values. In Fig. 4 we show the phase diagram together with the so-called Fisher-Widom lines that separate two distinct regions: the first, which is surrounding the consolute point of the mixture, is characterized by a monotonic decay of the correlation functions at large r -values, whereas the second by an oscillatory one. The second region is itself subdivided into two domains, each with different decay- and oscillation lengths. The Lifshitz lines drawn in Fig. 4 denote the locus of points on which the structure factors at $q = 0$ cross from having a local minimum to having a local maximum there.

The presence of two coexisting phases along points on the binodal implies that a free interface between the two will form when the chemical potentials μ_i , $i = 1, 2$ of the two phases attain appropriate values. DFT allows for a calculation of the density profiles across this interface. Let I and II be the two coexisting phases at the points (ρ^I, x^I) and (ρ^{II}, x^{II}) . Accordingly, the two components will have bulk densities $\rho_1^\alpha = (1 - x^\alpha)\rho^\alpha$ and $\rho_2^\alpha = x^\alpha\rho^\alpha$, $\alpha = I, II$, respectively. The density profiles across the free interface can be calculated by Eq. (42) with $V_{\text{ext}}^{(i)}(\mathbf{r}) = 0$,

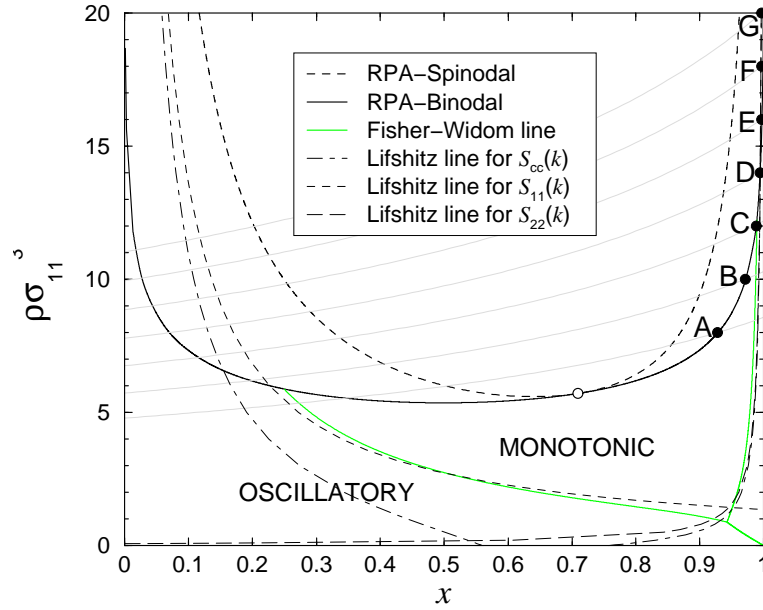


Fig. 4: The RPA-phase diagram along with the Fisher-Widom line (light solid line) and the Lifshitz lines of the various structure factors. The left hand branch of the FW line lies close to the Lifshitz line for $S_{11}(k)$ (short dashed line) while the right hand branch lies close to the Lifshitz line for $S_{22}(k)$ (long dashed line). The dash-dotted line is the Lifshitz line for the concentration structure factor $S_{cc}(k) = (1-x)^2 S_{11}(k) + x^2 S_{22}(k) - 2x(1-x)S_{12}(k)$. The points A-G on the right-hand branch of the binodal are located at total densities $\rho\sigma_{11}^3 = 8, 10, 12, 14, 16, 18$ and 20, at which the free interface density profiles will be calculated in what follows. The gray lines are RPA-isobars through the points A-G and their intersections with the left-hand branch of the binodal yield the state points coexisting with A-G. The open circle denotes the RPA-consolute point. (From Ref. [57]).

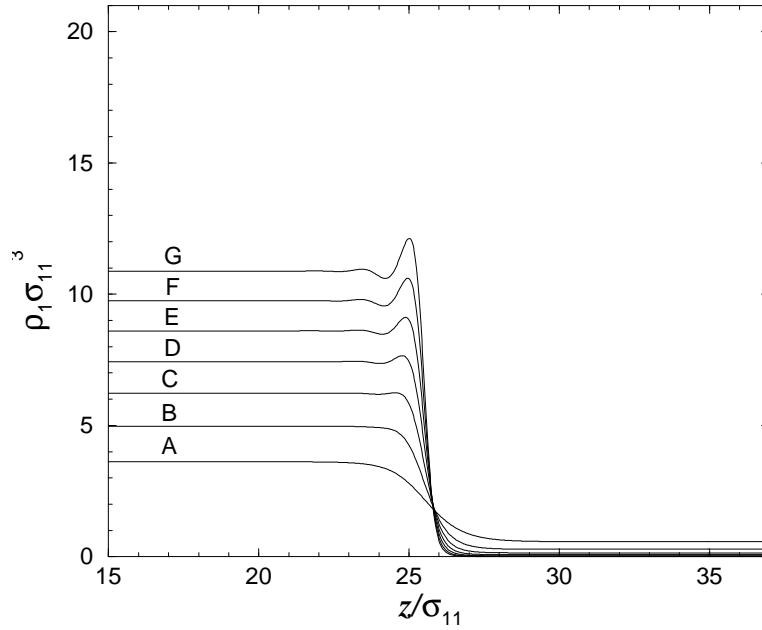


Fig. 5: The fluid-fluid interface density profiles of species 1, calculated at states A-G in the phase diagram, see Fig. 4. State A lies near the critical point and state G, for which the interface is much sharper, far away from the critical point. These states correspond to total bulk densities $\rho\sigma_{11}^3 = 8, 10, 12, 14, 16, 18$ and 20 in the phase rich in species 2. (From Ref. [57]).

under the boundary conditions:

$$\lim_{z \rightarrow -\infty} \rho_1(z) = \rho_1^I; \quad (46)$$

$$\lim_{z \rightarrow -\infty} \rho_2(z) = \rho_2^I; \quad (47)$$

$$\lim_{z \rightarrow +\infty} \rho_1(z) = \rho_1^{\text{II}}; \quad (48)$$

$$\lim_{z \rightarrow +\infty} \rho_2(z) = \rho_2^{\text{II}}, \quad (49)$$

i.e., forcing bulk phase I at $z \rightarrow -\infty$ and bulk phase II at $z \rightarrow \infty$.

Defining the shifted chemical potentials $\bar{\mu}_{1,2} \equiv \mu_{1,2} - 3 \ln(\Lambda_{1,2}/\sigma_{11})$, the explicit equations to be self-consistently solved for the density profiles, under the above-mentioned boundary conditions, read as:

$$k_B T \ln [\rho_1(z) \sigma_{11}^3] + \int d^3 r' [\rho_1(z') v_{11}(|\mathbf{r}' - \mathbf{r}|) + \rho_2(z') v_{12}(|\mathbf{r}' - \mathbf{r}|)] = \bar{\mu}_1; \quad (50)$$

$$k_B T \ln [\rho_2(z) \sigma_{11}^3] + \int d^3 r' [\rho_1(z') v_{12}(|\mathbf{r}' - \mathbf{r}|) + \rho_2(z') v_{22}(|\mathbf{r}' - \mathbf{r}|)] = \bar{\mu}_2, \quad (51)$$

where, in Cartesian coordinates, $\mathbf{r} = (x, y, z)$, $\mathbf{r}' = (x', y', z')$ and the profiles depend only in the third component of the position vector. The imposition of the boundary conditions forces then the occurrence of an interface. In Figs. 5 and 6 we show the density profiles for species 1 and 2 and for a number of different coexistence points, denoted A - G in Fig. 4. It can be seen that in the neighborhood of the consolute point the profiles are smooth, whereas as one moves

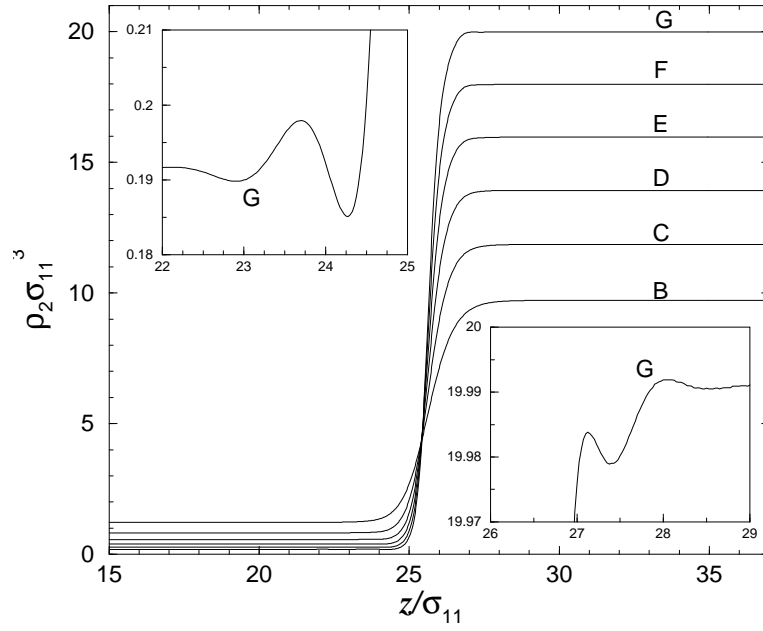


Fig. 6: Same as Fig. 5 but for species 2. The insets show magnified regions for state G. Note the oscillations on both sides of the interface. (From Ref. [57]).

away from it, density oscillations develop. The latter are most strongly visible for species 1 and they are present at the interface between the species 1-poor and the species 1-rich phase, on the species 1-rich side, see Fig. 5. The density oscillations for species 2 are much weaker and can be seen in the insets of Fig. 6. On the basis of the density profiles of the free fluid-fluid interface, the surface tension between the coexisting phases, γ , can be calculated, as

$$\gamma = \int_{-\infty}^{\infty} dz [P + \omega(z)], \quad (52)$$

where P is the pressure at coexistence and $\omega(z)$ is the grand potential *density* obtained from Eqs. (40) and (41) with the inhomogeneous density profiles of the free interface¹⁰ $\rho_i(z)$ and $V_{\text{ext}}^{(i)}(\mathbf{r}) = 0$, $i = 1, 2$.

4.4 Wetting

Another way to impose inhomogeneous density profiles in a fluid is to bring it in contact with a planar wall.¹¹ When a phase-separating mixture is forced to approach its binodal line in the presence of a planar wall, a variety of *wetting phenomena* can take place. In particular, the coexisting phase lying at the *opposite side* of the binodal can form a macroscopically thick layer on the wall *before* the binodal is reached. In this case, one says that the phase *wets* the wall and the layer thickness diverges on the binodal (complete wetting). The wetting scenarios,

¹⁰For homogeneous density profiles, it holds $\Omega = -PV$ and the integrand of Eq. (52) vanishes.

¹¹Of course, there are infinitely many ways to bring a fluid under geometric confinement by using spherical, cylindrical, arbitrarily shaped or topographically patterned walls. Here we limit ourselves to wetting on a *single, planar* wall.

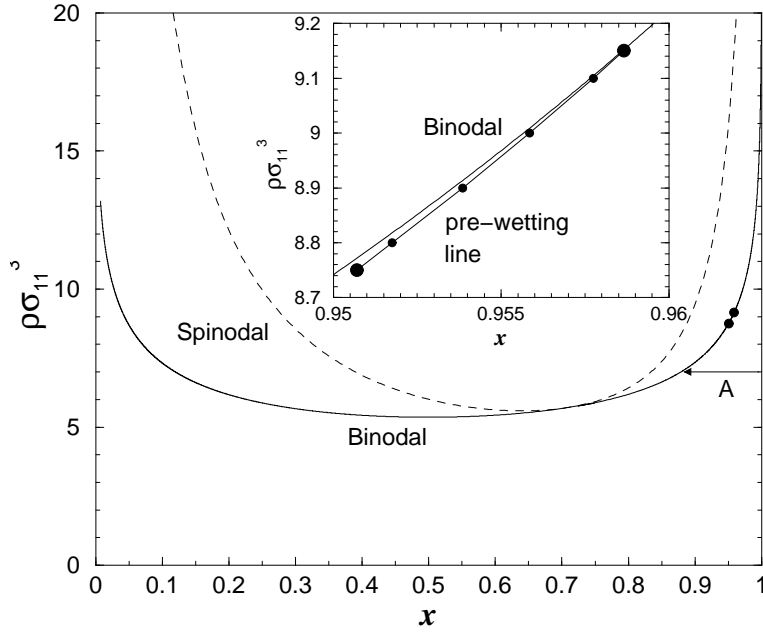


Fig. 7: The phase diagram obtained from the RPA (as in Figs. 3 and 4). The two filled circles show the location of the prewetting line. The upper point on the binodal is the wetting point where the prewetting line meets the binodal tangentially and the lower point is the consolute point at the end of the prewetting line. The inset shows the prewetting line at greater magnification. The horizontal path labeled A is that along which the density profiles in Fig. 8 are calculated. (From Ref. [57]).

which form indeed a distinct class of surface phase transitions, depend sensitively on the nature of interparticle and particle-wall interactions [59].

For the binary polymer system at hand, a hard wall can be placed at $z = 0$. The effective potentials of the central monomers of the chain with the walls, $V_{\text{ext}}^{(i)}(z)$, have been calculated by Jusufi *et al.* [47]. Whereas $V_{\text{ext}}^{(i)}(z)$ diverge for $z < 0$, for $z \geq 0$ they take the form:

$$\beta V_{\text{ext}}^{(i)}(z) = \Theta \begin{cases} -\ln\left(\frac{2z}{\sigma_{ii}}\right) - \left(\frac{4z^2}{\sigma_{ii}^2} - 1\right) \left(\psi_i - \frac{1}{2}\right) + \zeta_i & \text{for } 0 \leq z \leq \sigma_{ii}/2; \\ \zeta_i \text{erfc}(\kappa_i z) / \text{erfc}(\kappa_i \sigma_{ii}/2) & \text{for } z > \sigma_{ii}/2 \end{cases} \quad (53)$$

where $\text{erfc}(x) = 1 - \text{erf}(x)$ is the complementary error function, $\psi_i = (1 + \kappa_i^2 \sigma_{ii}^2/2)^{-1}$ is a parameter chosen to guarantee the continuity of the local osmotic pressure in the interior of the polymer, and

$$\zeta_i = \frac{2\sqrt{\pi}\psi_i}{\kappa_i \sigma_{ii}} \text{erfc}\left(\frac{\kappa_i \sigma_{ii}}{2}\right) \exp\left(\frac{\kappa_i^2 \sigma_{ii}^2}{4}\right). \quad (54)$$

The parameters κ_i and Θ have the values $\kappa_i = 1.16/\sigma_{ii}$ and $\Theta = 1.30$ [47].

The inhomogeneous density profiles imposed by the presence of the wall can be now calculated by solving the equations:

$$k_B T \ln [\rho_1(z) \sigma_{11}^3] + \int d^3 r' [\rho_1(z') v_{11}(|\mathbf{r}' - \mathbf{r}|) + \rho_2(z') v_{12}(|\mathbf{r}' - \mathbf{r}|)] = u_1(z); \quad (55)$$

$$k_B T \ln [\rho_2(z) \sigma_{11}^3] + \int d^3 r' [\rho_1(z') v_{12}(|\mathbf{r}' - \mathbf{r}|) + \rho_2(z') v_{22}(|\mathbf{r}' - \mathbf{r}|)] = u_2(z), \quad (56)$$

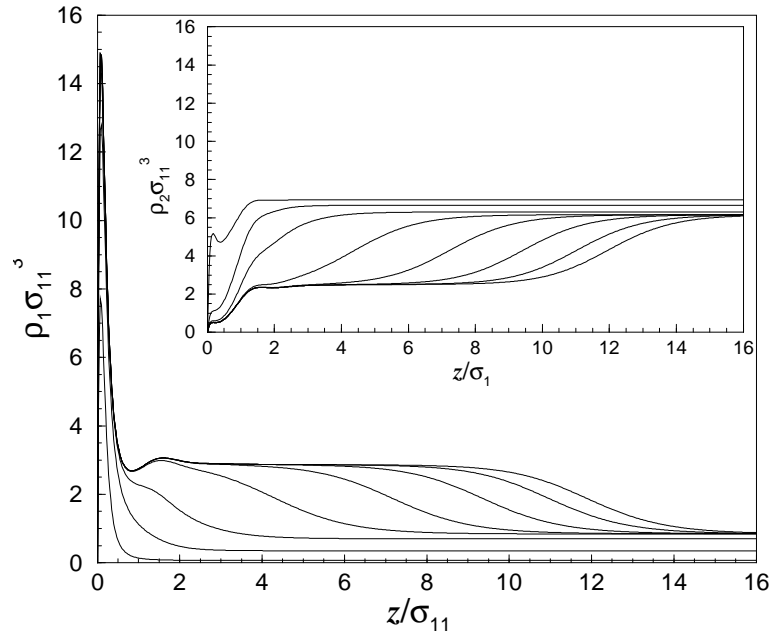


Fig. 8: The density profiles of species 1, the larger particles, adsorbed at a wall described by the potential (53), calculated along a path of constant total density, $\rho\sigma_{11}^3 = 7.0$, i.e., path A in Fig. 7. From left to right the profiles refer to $x = 0.99, 0.95, 0.9, 0.88, 0.879, 0.878955, 0.878951$ and 0.8789505 , where x is the concentration of species 2 and $x_{\text{coex}} = 0.87895019$. The thickness of the adsorbed film increases continuously as $x \rightarrow x_{\text{coex}}^+$, indicating complete wetting. The inset shows the density profiles of species 2 for the same values of x . Note that species 2 is depleted from the region adjoining the wall. (From Ref. [57]).

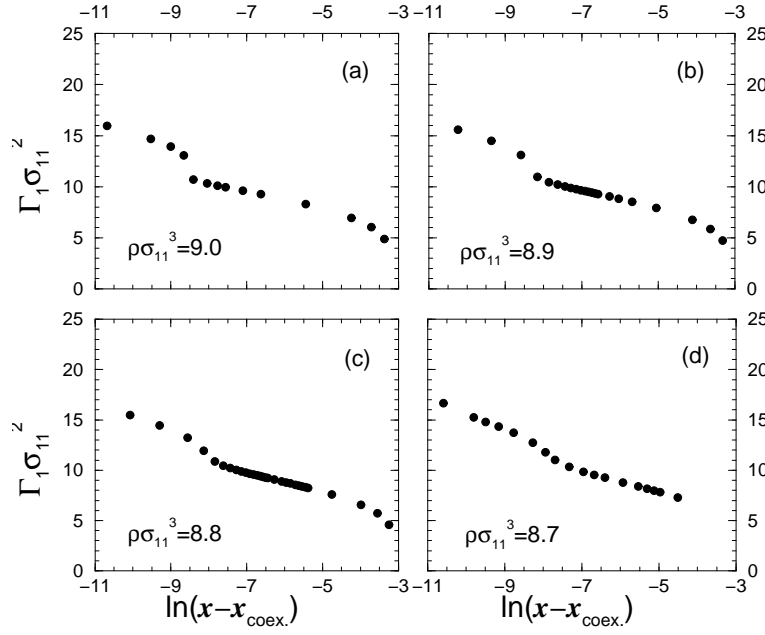


Fig. 9: Plots of the adsorption of species 1, Γ_1 , versus the logarithm of the deviation from bulk coexistence $\ln(x - x_{\text{coex.}})$, at constant total density ρ , for paths intersecting [(a)-(c)] and passing just below (supercritical) (d) the prewetting line. The jumps in (a)-(c) indicate the first-order prewetting transition. (From Ref. [57]).

where $u_i(z) \equiv \bar{\mu}_i - V_{\text{ext}}^{(i)}(z)$. Consider, then, moving along a path of constant total density ρ and decreasing x , such as path A in Fig. 7. The resulting density profiles are shown in Fig. 8. It can be seen that, as the binodal is approached, a thick film of a species 1-rich phase wets the wall, which diverges on the binodal: the system shows complete wetting.

The wetting behavior can be quantitatively analyzed by using the density profiles from DFT and looking at the *adsorption* of species 1 on the wall, defined as

$$\Gamma_1 = \int_0^\infty dz [\rho_1(z) - \rho_1], \quad (57)$$

where $\rho_1 = \rho_1(z \rightarrow \infty)$, i.e., the density of species 1 in the bulk.

In Fig. 9 we show adsorption curves at various different total densities ρ , varying the concentration x . It can be seen that there is a jump in the adsorption curves, which occurs before the coexistence curve is reached (at $x - x_{\text{coex.}} = 0$). In other words, there is a line of *first-order wetting transitions* traced by the points on the phase diagram for which the adsorption has a discontinuity. This so-called *prewetting line* is a short segment that is shown in the inset of Fig. 7. The lower end of the prewetting line, marked by the lower thick circle in the inset of Fig. 7, is the *wetting critical point*. This is a true surface critical point, similar in nature to the bulk critical points known from the theory of classical fluids. The upper end of the prewetting line, marked by the upper thick circle in the inset of Fig. 7, is the so-called *wetting point* and lies *on the binodal*. For paths of constant ρ lying higher than the location of the wetting, the adsorption of species 1 on the wall always remains finite, all the way to the binodal. For paths running below the wetting point, the adsorption always diverges on the binodal and a macroscopic, thick film of species 1 forms on the wall. If the path runs above the wetting critical point, intersecting the

prewetting line, then there is an adsorption jump on the latter. If not, i.e., if the path runs below the wetting critical point, then the adsorption Γ_1 grows smoothly as the binodal is approached and diverges right on it.

The above discussion demonstrates both the rich variety of surface-induced phase transitions and wetting behavior and the power of DFT to analyze these. The wetting scenarios can be modified at wish, leading to a disappearance of the prewetting line or to its displacement on the opposite side of the binodal, by suitable modifications of the wall potentials $V_{\text{ext}}^{(i)}(z)$.

4.5 Crystallization

The density inhomogeneities discussed in the preceding sections pale in comparison with the ones arising in a crystalline solid. In this case, whereas the one-particle density is extremely high in the neighborhood of the lattice sites, the strong localization of the particles around the latter causes the density at the interstitial regions to be extremely low. The peak value of the density on the lattice site, compared to its value in the mid-point between the nearest neighbors can differ by as many as 50 orders of magnitude! It is without a doubt a most challenging task for DFT to be able to make quantitative predictions on the structure and stability of crystalline solids, which spontaneously form under the appropriate thermodynamic conditions (density and temperature) and without the presence of external potentials. The prototype system for crystallization is the hard-sphere fluid, for which a number of functionals that predict crystallization have been developed [39]. Hard spheres freeze into a face-centered cubic (fcc) lattice at packing fraction $\eta \cong 0.49$ [60–65]. Coulomb systems, and in particular the one-component plasma (OCP) are another common example of systems for which density functionals leading to freezing have been developed [66]. Contrary to hard spheres, the OCP freezes into a body-centered cubic (bcc) lattice at sufficiently strong Coulomb couplings.

To demonstrate the power of DFT and to stay within the realm of the RPA-functional for ultra-soft potentials, we discuss here a recent study on the freezing transition of Yukawa systems [67]. These consist of point particles that interact by means of the purely repulsive potential:

$$v(r) = \frac{\epsilon \exp(-\lambda r)}{\lambda r}, \quad (58)$$

where $\epsilon > 0$ is an energy parameter and λ is the inverse decay length: for large values of λ the potential is strongly screened. Eq. (58) describes the screened Coulomb interaction of pointlike charged entities. Evidently, the potential of Eq. (58) fulfills the condition (37).

The one-particle density $\rho(\mathbf{r})$ of the crystals possesses evidently the discrete translational and point symmetries dictated by the underlying Bravais lattice; the latter is spanned by the Bravais lattice vectors set $\{\mathbf{R}_i\}$. The localization of the particles around crystal sites is adequately parametrized by modeling the density by a sum of normalized Gaussian profiles centered around the lattice sites, viz.

$$\rho(\mathbf{r}) = \left(\frac{\alpha}{\pi}\right)^{3/2} \sum_{\mathbf{R}_i} \exp[-\alpha(\mathbf{r} - \mathbf{R}_i)^2]. \quad (59)$$

The parameter α expresses the degree of localization of the ‘Gaussian orbitals’ around the lattice sites: whereas for $\alpha = 0$ a uniform profile results, for $\alpha \rightarrow \infty$ the Gaussians reduce to Dirac-delta peaks.

With the modeling of Eq. (59), the free energy becomes, at given average density and temperature and for any given Bravais lattice, a function of α . The latter is used as a variational

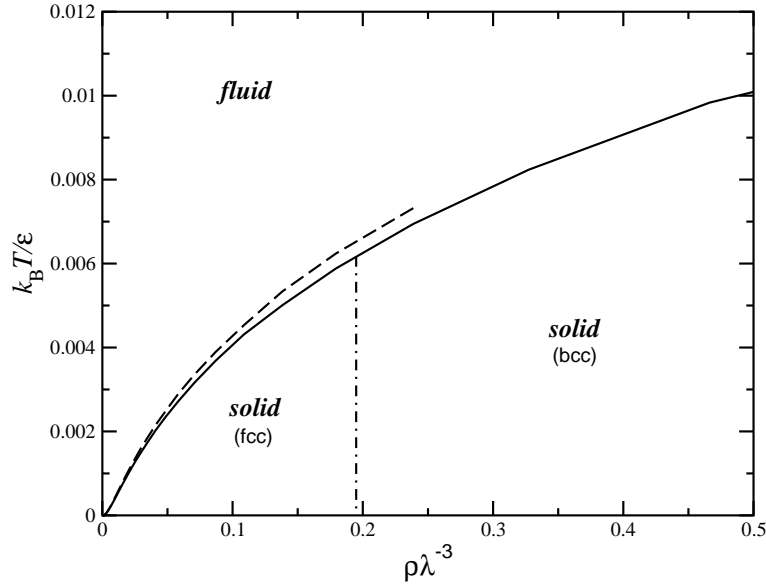


Fig. 10: The phase diagram of the Yukawa fluid, as predicted by the density-functional approach described in the text. (Redrawn from Ref. [67]).

parameter and the minimum of $F[\rho]$ at fixed average density is sought. For the case of nonoverlapping Gaussians, the ideal free energy of Eq. (33) can be extremely well approximated by the analytical expression

$$F_{\text{id}}(\alpha) = N k_{\text{B}} T \left[\frac{3}{2} \ln \left(\frac{\alpha \Lambda^2}{\pi} \right) - \frac{5}{2} \right]. \quad (60)$$

The RPA-excess free energy functional of Eq. (38) has to be slightly modified for the case at hand, in the sense that all terms with $\mathbf{R}_i = \mathbf{R}_j$ in the density products must be excluded to avoid self-interaction terms. It then takes the form

$$F_{\text{ex}}(\alpha) = \frac{1}{2} \sum_{i \neq j} \frac{1}{(2\pi)^3} \int d^3 k \exp(i\mathbf{k} \cdot \mathbf{R}_{ij}) \hat{v}(k) \exp[-k^2/(2\alpha)], \quad (61)$$

where $\mathbf{R}_{ij} = \mathbf{R}_i - \mathbf{R}_j$, and $\hat{v}(k)$ is the Fourier transform of the pair potential. Whereas the ideal term, Eq. (60), grows with α and thus favors delocalization, the excess term, Eq. (61), attains its minimum for $\alpha \rightarrow \infty$ and favors localization.¹² The competition between the two gives rise to a stable minimum at $\alpha \neq 0$, corresponding to a mechanically stable fluid.¹³

Given the free energy of the crystals from DFT, one can combine it with the free energy of the fluid, calculated, e.g., by the methods described in Sec. 3, to draw the phase diagram of the system. A simpler (but less accurate) way is to determine from DFT the so-called *Lindemann ratio* L : this is the ratio of the root-mean-square of the displacement of a particle from its lattice site over the nearest neighbor distance and directly follows from the value of the localization parameter α . Empirically, crystals melt when L exceeds 10%. In this way, the phase diagram of Fig. 10 can be obtained for the Yukawa system. Clearly, DFT can predict freezing as well as the polymorphic fcc \rightarrow bcc structural phase transformation that takes place as the density grows.

¹²It can be easily seen that for $\alpha \rightarrow \infty$ this term reduces to $(1/2) \sum_{i \neq j} v(|\mathbf{R}_i - \mathbf{R}_j|)$, the *lattice sum* of the crystal that corresponds to the internal energy of N particles lying motionless on the lattice sites.

¹³Usually, this minimum occurs at a value of α large enough to justify the approximations involved in deriving Eq. (60).

5 Summary and conclusions

We have presented a rather concise overview of the methods employed in modern statistical mechanical approaches to explore and understand the properties of colloidal suspensions. The paper has focused exclusively on theoretical approaches, putting particular emphasis on density functional theory. A host of other possibilities also exist: microscopic or coarse-grained computer simulations are a tool that has been developed and constantly refined in the recent years. Experimentally, scattering methods but also direct observations in real space, as well as manipulations of the colloids using external fields, also belong to the arsenal of tools at hand used to explore this vast and exciting research field.

Acknowledgments

I wish to thank Andrew Archer for sending me a copy of Ref. [67] prior to publication and for helpful discussions.

Appendices

A Functionals and functional differentiation

The notion of a function of a finite number of variables is familiar from elementary calculus.¹⁴ A function $f(x_1, x_2, \dots, x_n)$ is a mapping or a rule that assigns a single number (or a vector) to an ordered array of variables (x_1, x_2, \dots, x_n) . The following are examples of functions of one, two, and n variables, respectively:

$$f(x) = x^2; \quad g(x_1, x_2) = \sin(x_1 + x_2); \quad h(x_1, x_2, \dots, x_n) = \sum_{i=1}^n \exp(x_i). \quad (62)$$

A **functional** is a generalization of this idea. The argument of a functional is an *entire function* f of one or many variables and a number $I[f]$ is assigned to it. A simple example of a functional is

$$I[f] = \int_{-1}^1 f(x) dx. \quad (63)$$

Here, the result of the integration depends on the whole function $f(x)$, hence I is a *functional* of $f(x)$, denoted by the square brackets, $I[f]$. There are numerous examples of functionals already encountered in undergraduate Physics lectures. Two particular examples are the action $S[\mathcal{L}]$ of a classical particle, which is a functional of the Lagrangian $\mathcal{L}(q, \dot{q})$, which is itself a *function* of the generalized coordinate q and velocity \dot{q} . Another is the total energy of an electromagnetic field, $W[\mathbf{E}, \mathbf{B}; t] = 1/(8\pi) \int d^3r [|\mathbf{E}(\mathbf{r}, t)|^2 + |\mathbf{B}(\mathbf{r}, t)|^2]$, which is again a *functional* of the full spatiotemporal electric and magnetic fields $\mathbf{E}(\mathbf{r}, t)$ and $\mathbf{B}(\mathbf{r}, t)$ and at the same time a *function* of the time t .

¹⁴Parts of this Appendix have been inspired by the discussion in Ref. [68].

In statistical mechanics, functionals are again omnipresent. One known example from statistical field theory is the famous *Landau-Ginzburg free energy* $F_{\text{LG}}[\phi]$:

$$F_{\text{LG}}[\phi] = \int d^d r \left[\frac{K}{2} |\nabla \phi(\mathbf{r})|^2 + \frac{\mu}{2!} \phi^2(\mathbf{r}) + \frac{\lambda}{4!} \phi^4(\mathbf{r}) \right], \quad (64)$$

which describes the fluctuations of a coarse-grained scalar field $\phi(\mathbf{r})$ in d -dimensional space and assigns a statistical weight $W[\phi] \propto \exp\{-F_{\text{LG}}[\phi]\}$ to each particular field realization. The free energy functional $F[\rho]$ that plays the central role in density functional theory is just another example, for which a whole, spatially-dependent function $\rho(\mathbf{r})$ is mapped onto a single scalar quantity $F[\rho]$. In density functional theory (and in statistical field theory), more complicated situations can arise, in which a functional depends not only on the density field $\rho(\mathbf{r})$ but is also a *function* of a whole collection of spatial coordinates $(\mathbf{r}_1, \mathbf{r}_2, \dots, \mathbf{r}_n)$. Indeed, the n -body direct correlation function $-k_B T c^{(n)}$, which is defined as the n -th functional derivative of the excess free energy functional $F_{\text{ex}}[\rho]$ with respect to the density is precisely a function of n spatial coordinates and a functional of $\rho(\mathbf{r})$. It is customary to denote such ‘mixed’ objects as

$$c^{(n)} = c^{(n)}(\mathbf{r}_1, \mathbf{r}_2, \dots, \mathbf{r}_n; [\rho]), \quad (65)$$

i.e., to use parentheses in order to emphasize their character as functions of the variables $(\mathbf{r}_1, \mathbf{r}_2, \dots, \mathbf{r}_n)$ and additional square brackets to remind their functional dependence on the entire density field $\rho(\mathbf{r})$. The notation in Eq. (65) above thus means: for each field $\rho(\mathbf{r})$, $c^{(n)}$ is a different function of $(\mathbf{r}_1, \mathbf{r}_2, \dots, \mathbf{r}_n)$. A very simple, concrete example of such a mixed object is given below:

$$G(\mathbf{s}; [\rho]) = \int d^3 r f(\rho(\mathbf{r})) K(\mathbf{r}, \mathbf{s}), \quad (66)$$

which is a function of \mathbf{s} and a functional of $\rho(\mathbf{r})$ for a given integration kernel $K(\mathbf{r}, \mathbf{s})$. Note that the quantity $f(\rho(\mathbf{r}))$ appearing in the integrand is a *function* of $\rho(\mathbf{r})$, in the sense that its value depends only on the *local* value of the field at the position \mathbf{r} and *not* on the entire density profile. Formally, local functions of the density can still be looked upon as functionals through the choice $K(\mathbf{r}, \mathbf{s}) = \delta(\mathbf{r} - \mathbf{s})$ in Eq. (66) above.

We now proceed with the definition of the *functional derivative* of a functional $F[\rho]$ with respect to the density. This quantity ought to tell us what happens to F if we change the profile $\rho(\mathbf{r})$ locally at the position \mathbf{r}_0 . In analogy with the usual derivative, its functional counterpart is defined as

$$\frac{\delta F}{\delta \rho(\mathbf{r}_0)} \equiv \lim_{\epsilon \rightarrow 0} \frac{F[\rho(\mathbf{r}) + \epsilon \delta(\mathbf{r} - \mathbf{r}_0)] - F[\rho(\mathbf{r})]}{\epsilon} = G(\mathbf{r}_0; [\rho]). \quad (67)$$

Evidently, the result of a functional differentiation depends on the entire profile $\rho(\mathbf{r})$ and on the position \mathbf{r}_0 on which the local density variation is taken. It is, therefore, a mixed object, a *function* of \mathbf{r}_0 and a *functional* of $\rho(\mathbf{r})$, as the notation manifests.

The simplest functionals to differentiate are the local ones mentioned above. For those, it follows directly from the definition (67) that the functional derivative is closely related to the usual derivative, viz.

$$\frac{\delta f(\rho(\mathbf{r}))}{\delta \rho(\mathbf{r}_0)} = \delta(\mathbf{r} - \mathbf{r}_0) \left. \frac{df(s)}{ds} \right|_{s=\rho(\mathbf{r})}. \quad (68)$$

As a corollary we obtain the useful identity

$$\frac{\delta\rho(\mathbf{r})}{\delta\rho(\mathbf{r}_0)} = \delta(\mathbf{r} - \mathbf{r}_0). \quad (69)$$

Another useful rule for functional differentiation is the generalization of the *chain rule* of usual differentiation. Suppose that F is a functional of the function g , $F = F[g]$, and that the function g is itself a functional of f , $g = g(\mathbf{r}; [f])$. Now suppose that f changes. This will cause g to change and this change will propagate to F . It is therefore legitimate to regard $F[g]$ also as a functional $\tilde{F}[f]$ and to ask what the functional derivative of \tilde{F} with respect to f is. The answer is provided by the *functional chain rule* below:

$$\frac{\delta\tilde{F}[f]}{\delta f(\mathbf{r}_0)} = \int d^3r \frac{\delta F[g]}{\delta g(\mathbf{r}; [f])} \frac{\delta g(\mathbf{r}; [f])}{\delta f(\mathbf{r}_0)}. \quad (70)$$

Let now $I[f]$ be the functional defined in Eq. (63) and let us additionally define two simple functionals of the density $\rho(\mathbf{r})$ as:

$$G[\rho] = \int d^3r \rho(\mathbf{r}) \{ \ln [\rho(\mathbf{r})\Lambda^3] - 1 \}; \quad (71)$$

$$F[\rho] = \frac{1}{2} \int \int d^3x d^3y \rho(\mathbf{x}) \rho(\mathbf{y}) v(|\mathbf{x} - \mathbf{y}|). \quad (72)$$

Using the rules given above, the reader is asked to prove the following relations:

$$1. \quad \frac{\delta I[f]}{\delta f(x_0)} = \begin{cases} 1 & \text{if } |x_0| < 1; \\ 0 & \text{otherwise.} \end{cases} \quad (73)$$

$$2. \quad \frac{\delta I[f^2]}{\delta f(x_0)} = \begin{cases} 2f(x_0) & \text{if } |x_0| < 1; \\ 0 & \text{otherwise.} \end{cases} \quad (74)$$

$$3. \quad \frac{\delta G[\rho]}{\delta \rho(\mathbf{r}_0)} = \ln [\rho(\mathbf{r}_0)\Lambda^3]. \quad (75)$$

$$4. \quad \frac{\delta F[\rho]}{\delta \rho(\mathbf{z})} = \int d^3x \rho(\mathbf{x}) v(|\mathbf{x} - \mathbf{z}|). \quad (76)$$

$$5. \quad \frac{\delta^2 F[\rho]}{\delta \rho(\mathbf{z}) \delta \rho(\mathbf{w})} = v(|\mathbf{z} - \mathbf{w}|). \quad (77)$$

$$6. \quad \frac{\delta^n F[\rho]}{\delta \rho(\mathbf{r}_1) \delta \rho(\mathbf{r}_2) \cdots \delta \rho(\mathbf{r}_n)} = 0 \text{ for } n \geq 3. \quad (78)$$

References

- [1] W. B. Russel, D. A. Saville, and W. R. Schowalter, *Colloidal Dispersions*, Cambridge University Press, Cambridge, 1989.
- [2] R. J. Hunter, *Foundations of Colloid Science*, volume I, Clarendon Press, Oxford, 1986.
- [3] J. W. Vanderhoff, H. J. van den Hul, R. J. M. Tausk, and J. T. G. Overbeek, in *Clean Surfaces: Their Preparation and Characterization for Interfacial Studies*, Dekker, New York, 1970, ed. by G. Goldfinger.

- [4] J. W. Goodwin, J. Hearn, C. C. Ho, and R. H. Otewill, *Br. Polymer J.* **5**, 347 (1973).
- [5] R. K. Iler, in *Surface and Colloid Science*, Wiley, New York, 1973, Vol. 5, ed. by E. Matijevic.
- [6] R. K. Iler, in *The Chemistry of Silica*, Wiley, New York, 1979.
- [7] K. E. J. Barrett, *Dispersion Polymerization in Organic Media*, Wiley, London, 1975.
- [8] L. Antl, J. W. Goodwin, R. D. Hill, R. H. Otewill, S. M. Owens, S. Papworth, and J. A. Waters, *Colloids and Surfaces* **17**, 67 (1986).
- [9] P. N. Pusey, in *Les Houches, Session LI, Liquids, Freezing and Glass Transition*, North-Holland, Amsterdam, 1991, ed. by J.-P. Hansen, D. Levesque and J. Zinn-Justin.
- [10] J.-P. Hansen and H. Löwen, *Ann. Rev. Phys. Chem.* **51**, 209 (2000).
- [11] L. Belloni, *J. Phys.: Condens. Matter* **12**, R549 (2000).
- [12] G. S. Grest, L. J. Fetters, J. S. Huang, and D. Richter, *Adv. Chem. Phys.* **XCIV**, 67 (1996).
- [13] C. N. Likos, H. Löwen, M. Watzlawek, B. Abbas, O. Jucknischke, J. Allgaier, and D. Richter, *Phys. Rev. Lett.* **80**, 4450 (1998).
- [14] M. Watzlawek, C. N. Likos, and H. Löwen, *Phys. Rev. Lett.* **82**, 5289 (1999).
- [15] W. G. McMillan and J. E. Mayer, *J. Chem. Phys.* **13**, 276 (1945).
- [16] J. G. Kirkwood and F. P. Buff, *J. Chem. Phys.* **19**, 774 (1951).
- [17] W. van Megen and I. Snook, *Adv. Coll. Interface Sci.* **21**, 119 (1984).
- [18] C. N. Likos, *Phys. Rep.* **348**, 267 (2001).
- [19] M. Dijkstra, R. van Roij, and R. Evans, *Phys. Rev. E* **59**, 5744 (1999).
- [20] R. van Roij and J.-P. Hansen, *Phys. Rev. Lett.* **79**, 3082 (1997).
- [21] R. van Roij, M. Dijkstra, and J.-P. Hansen, *Phys. Rev. E* **59**, 2010 (1999).
- [22] J.-P. Hansen and I. R. McDonald, *Theory of Simple Liquids*, Academic Press, London, second edition, 1986.
- [23] J. S. Higgins and H. C. Benoît, *Polymers and Neutron Scattering*, Clarendon Press, Oxford, 1994.
- [24] Y. Rosenfeld and N. W. Ashcroft, *Phys. Rev. A* **20**, 1208 (1979).
- [25] F. A. Rogers and D. A. Young, *Phys. Rev. A* **30**, 999 (1984).
- [26] P. Hutchinson and W. R. Conkie, *Mol. Phys.* **24**, 567 (1972).
- [27] D. S. Hall and W. R. Conkie, *Mol. Phys.* **40**, 907 (1980).
- [28] L. Verlet, *Mol. Phys.* **42**, 1291 (1981).

- [29] T. Munakata, *Phys. Rev. E* **50**, 2347 (1994).
- [30] J. Araki and T. Munakata, *Phys. Rev. E* **52**, 2577 (1995).
- [31] D. S. Dean, *J. Phys. A* **29**, L613 (1996).
- [32] U. M. B. Marconi and P. Tarazona, *J. Chem. Phys.* **110**, 8032 (1999).
- [33] A. J. Archer and M. Rauscher, *J. Phys. A* **37**, 9325 (2004).
- [34] J. Dzubiella and C. N. Likos, *J. Phys.: Condens. Matter* **15**, L147 (2003).
- [35] A. J. Archer and R. Evans, *J. Chem. Phys.* **121**, 4246 (2004).
- [36] M. Rex, H. Löwen, and C. N. Likos, *Phys. Rev. E* **72**, 021404 (2005).
- [37] R. Evans, *Adv. Phys.* **28**, 143 (1979).
- [38] T. V. Ramakrishnan and M. Yussouff, *Phys. Rev. B* **19**, 2775 (1979).
- [39] R. Evans, in *Fundamentals of Inhomogeneous Fluids*, Marcel Dekker, New York, 1992, ed. by D. Henderson.
- [40] Y. Rosenfeld, *J. Chem. Phys.* **98**, 8126 (1993).
- [41] M. Schmidt, *J. Phys.: Condens. Matter* **15**, S101 (2003).
- [42] A. A. Louis, P. G. Bolhuis, J.-P. Hansen, and E. J. Meijer, *Phys. Rev. Lett.* **85**, 2522 (2000).
- [43] M. Konieczny, C. N. Likos, and H. Löwen, *J. Chem. Phys.* **121**, 4913 (2004).
- [44] C. N. Likos, M. Schmidt, H. Löwen, M. Ballauff, D. Pötschke, and P. Lindner, *Macromolecules* **34**, 2914 (2001).
- [45] C. N. Likos, S. Rosenfeldt, N. Dingenouts, M. Ballauff, P. Lindner, N. Werner, and F. Vögtle, *J. Chem. Phys.* **117**, 1869 (2002).
- [46] I. O. Götze, H. M. Harreis, and C. N. Likos, *J. Chem. Phys.* **120**, 7761 (2004).
- [47] A. Jusufi, J. Dzubiella, C. N. Likos, C. von Ferber, and H. Löwen, *J. Phys.: Condens. Matter* **13**, 6177 (2001).
- [48] D. Gottwald, C. N. Likos, G. Kahl, and H. Löwen, *Phys. Rev. Lett.* **92**, 068301 (2004).
- [49] D. Gottwald, C. N. Likos, G. Kahl, and H. Löwen, *J. Chem. Phys.* **122**, 074903 (2005).
- [50] A. Jusufi, C. N. Likos, and H. Löwen, *Phys. Rev. Lett.* **88**, 018301 [1] (2002).
- [51] A. Jusufi, C. N. Likos, and H. Löwen, *J. Chem. Phys.* **116**, 11011 (2002).
- [52] A. Lang, C. N. Likos, M. Watzlawek, and H. Löwen, *J. Phys.: Condens. Matter* **12**, 5087 (2000).
- [53] C. N. Likos, A. Lang, M. Watzlawek, and H. Löwen, *Phys. Rev. E* **63**, 031206 (2001).

- [54] A. A. Louis, P. G. Bolhuis, and J.-P. Hansen, *Phys. Rev. E* **62**, 7961 (2000).
- [55] A. J. Archer and R. Evans, *Phys. Rev. E* **64**, 041501 (2001).
- [56] A. J. Archer and R. Evans, *J. Phys.: Condens. Matter* **14**, 1131 (2002).
- [57] A. J. Archer, C. N. Likos, and R. Evans, *J. Phys.: Condens. Matter* **14**, 12031 (2002).
- [58] L. Acedo and A. Santos, *Phys. Lett. A* **323**, 427 (2004).
- [59] S. Dietrich, in *Phase Transitions and Critical Phenomena*, Academic, London, 1988, ed. by C. Domb and J. L. Lebowitz, Vol. 12, p. 1.
- [60] B. J. Alder and T. E. Wainwright, *J. Chem. Phys.* **27**, 1208 (1957).
- [61] W. W. Wood and J. D. Jacobson, *J. Chem. Phys.* **27**, 1207 (1957).
- [62] B. J. Alder, W. G. Hoover, and D. A. Young, *J. Chem. Phys.* **49**, 3688 (1968).
- [63] W. G. Hoover and F. H. Ree, *J. Chem. Phys.* **49**, 3609 (1968).
- [64] A. D. J. Haymet and D. Oxtoby, *J. Chem. Phys.* **84**, 1769 (1986).
- [65] P. Bolhuis, D. Frenkel, S. C. Mau, and D. A. Huse, *Nature* **388**, 235 (1997).
- [66] C. N. Likos and N. W. Ashcroft, *Phys. Rev. Lett.* **69**, 316 (1992).
- [67] A. J. Archer, *Phys. Rev. E* **72**, 051501 (2005).
- [68] J. J. Binney, N. J. Dowrick, A. J. Fischer, and M. E. J. Newman, *The Theory of Critical Phenomena: An Introduction to the Renormalization Group*, Oxford, 1992.